Original scientific paper

EVOLUTION OF THE CARBON NANOTUBE BUNDLE STRUCTURE UNDER BIAXIAL AND SHEAR STRAINS

Leysan Kh. Rysaeva[1], Dmitry V. Bachurin[2], Ramil T. Murzaev[1], Dina U. Abdullina[1], Elena A. Korznikova[1,3], Radik R. Mulyukov[1,3], Sergey V. Dmitriev[3,4]

[1]Institute for Metals Superplasticity Problems of the Russian Academy of Sciences, Russia
[2]Institute for Applied Materials, Karlsruhe Institute of Technology, Germany
[3]Ufa State Petroleum Technological University, Russia
[4]National Research Tomsk State University, Russia

Abstract. *Close packed carbon nanotube bundles are materials with highly deformable elements, for which unusual deformation mechanisms are expected. Structural evolution of the zigzag carbon nanotube bundle subjected to biaxial lateral compression with the subsequent shear straining is studied under plane strain conditions using the chain model with a reduced number of degrees of freedom. Biaxial compression results in bending of carbon nanotubes walls and formation of the characteristic pattern, when nanotube cross-sections are inclined in the opposite directions alternatively in the parallel close-packed rows. Subsequent shearing up to a certain shear strain leads to an appearance of shear bands and vortex-like displacements. Stress components and potential energy as the functions of shear strain for different values of the biaxial volumetric strain are analyzed in detail. A new mechanism of carbon nanotube bundle shear deformation through cooperative, vortex-like displacements of nanotube cross sections is reported.*

Key Words: *Carbon Nanotube Bundle, Plane Strain Conditions, Lateral Compression, Shear Deformation, Deformation Mechanisms*

1. Introduction

In nature, there are many allotropic modifications of carbon with different physical properties. One of such modifications is carbon nanotube (CNT), which is but a rolled sheet of graphene. The peculiarity of CNTs is that they interact rather weakly with each other and can form CNT bundles [1-4]. The interest in CNTs is primarily due to their unique mechanical properties such as very high tensile strength, high Young's modulus, and ultimate fracture strain [5-8]. CNTs are flexible and lightweight and have good thermal and electric conductivity. Mechanical applications of CNTs include high-strength ropes [2,9], fibers [10-14], polymer- and metal-matrix composites [15-17], solid lubricants [17-20], and many others.

Tensile [2,9-14] and compressive [21-28] behavior of vertically aligned CNT brushes and forests have been most extensively studied experimentally. Straining of vertically aligned CNTs implies deformation along their axis, while straining of horizontally aligned CNTs means deformation normal to their axis. Lateral compression of isolated CNTs or CNT bundles has not been widely studied yet [29-33]. It should be noted that the methods of winding, drawing, micromechanical rolling, and shear pressing [34-37] can be applied to obtaining horizontally aligned CNT bundles from the vertically aligned ones. It has been revealed that CNT bundles can deform elastically up to hydrostatic pressure of 1.5 GPa, and the hydrostatic deformation of CNT lattice is reversible up to 4 GPa [38]. Karmakar and co-authors have demonstrated that deformation of CNT bundles under non-hydrostatic pressure is reversible (elastic) at stresses below 5 GPa [39].

In the last two decades, considerable attention has been paid to computer modeling of the mechanical properties of CNT bundles for a better understanding of their properties and deformation mechanisms. Since a nanotube bundle can be represented as a material with highly deformable elements, new deformation mechanisms different from those typical for conventional materials can be expected. In particular, transformation of vertically aligned CNT forest into a horizontally aligned one under pressure has been studied *via* mesoscopic modeling [40,41]. Different morphological patterns of CNTs subjected to large deformations have been revealed by means of continuum shell model [42]. The rigidity of CNT crystal does not decrease with increasing CNT diameter [1]. Authors [43-45] have found that CNTs can exist in two stable configurations (circular and collapsed ones) depending on their diameter. Nonlinear coarse-grained potentials specially developed for CNTs have allowed studying the mechanical response and failure of CNT bundles [46]. The chain model developed in Ref. [47] has been applied successfully to the investigation of structure and properties of carbon nanoribbons [47-51] and dynamics of surface ripplocations [52]. Recently, the chain model has been used for simulation of evolution of CNT bundle structure under both lateral uniaxial and biaxial compression [53-55].

The present work is devoted to a study of structural evolution of zigzag CNT bundle under biaxial compression with the subsequent shear straining using the chain model [47,53]. The latter uses a reduced number of degrees of freedom but at the same time gives at least one order of magnitude acceleration of computations without loss of accuracy, in comparison with full atomistic modeling under plane strain conditions. Despite the fact that the chain model [47,53] can be applied for various CNTs, here we restrict ourselves to the consideration of only single-walled CNTs of equal diameter.

2. MODEL AND COMPUTATIONAL DETAILS

The computational cell of the modeled bundle has a parallelogram shape and contains 1080 zigzag CNTs (30 horizontal layers and 36 vertical layers) of equal diameter aligned along the z-axis. For clarity, Fig. 1 represents only a part of the computational cell (two horizontal layers and two vertical layers). Each CNT consists of 60 carbon atoms. Total number of atoms in the cell is $N=60\times30\times36=64800$. Periodic boundary conditions are applied along the two (x,y) Cartesian directions, i.e., infinitely elongated along the z-axis CNTs are considered.

Lateral compression of the CNT bundle is applied using plane strain conditions, namely when each carbon atom stays rigidly in "its own" atomic row along the z-axis, but can move freely along the (x,y) plane. Thus, each atom has only two degrees of freedom, which allows us to reduce the dimensionality of the problem from three-dimensional to two-dimensional one.
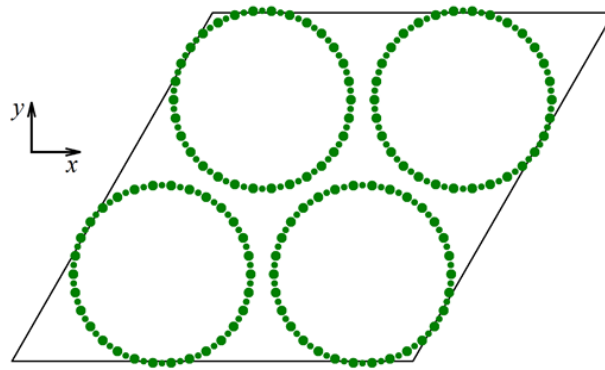
Fig. 1 Geometry of the computational cell. Only two horizontal layers and two vertical layers are presented for clarity, while in simulation 30 horizontal layers and 36 vertical layers are used. Carbon atoms in the upper row are indicated by large green circles, and those in the lower row are indicated by small circles. Each CNT contains 60 carbon atoms. The CNT cross-sections represent a triangular lattice

The following geometrical parameters for the model of CNT bundle are chosen. The valence bond length in graphene is $\rho=1.418$ Å. The distance between neighboring atomic rows in the zigzag CNT is $a=1.228$ Å. The CNT diameter is $D=23.46$ Å and the equilibrium distance between the neighboring CNT walls is $d=3.30$ Å. Thus, the centers of neighboring CNTs are at the distance of $A=D+d=26.76$ Å.

The Hamiltonian describing the interaction between carbon atoms includes the four terms, namely

$$H=K+U_B+U_A+U_{VdW}. \tag{1}$$

Here the first term, K, gives the kinetic energy of the carbon atoms, U_B stands for the energy of valence bonds, U_A is the energy of valence angles, and U_{VdW} is the energy of van der Waals interactions between CNTs. The model parameters were calculated based

on the interatomic potential developed for sp^2-carbon by Savin *et al*. [56] and further applied for investigation of various phenomena [56-61].

The initially constructed CNT bundle is subjected to relaxation in order to obtain minimum energy configuration. A biaxial compression (with $\varepsilon_{xx}<0$ and $\varepsilon_{yy}<0$) is applied by a strain increment of $\Delta\varepsilon_{xx}=\Delta\varepsilon_{yy}=-0.0025$, which is followed by giving to carbon atoms small random displacements in the range from -10^{-6} to 10^{-6} Å along the *x*- and *y*-axes and further minimization of potential energy $U=U_B+U_A+U_{VdW}$. The relaxation of the system is stopped, when the absolute value of the maximal force acting on atoms becomes less than 10^{-10} eV/Å. This biaxially strained structure is deformed again by applying subsequently a shear strain up to $\gamma=0.30$ with the step of $\Delta\gamma=0.01$. The strain state of deformed system is thus characterized by two parameters: the absolute value of the volumetric strain,

$$|\theta|=|\varepsilon_{xx}+\varepsilon_{yy}|, \tag{2}$$

and shear strain, γ. In the present study, no thermal effects are taken into consideration. For further details related to the simulation setup and construction of the Hamiltonian of the chain model, we refer the reader to our previous publications [53-55].

3. SIMULATION RESULTS AND DISCUSSION

Firstly, structural evolution of the CNT bundle under simple biaxial compression is considered, and, secondly, biaxial compression followed by a shear strain is analyzed.
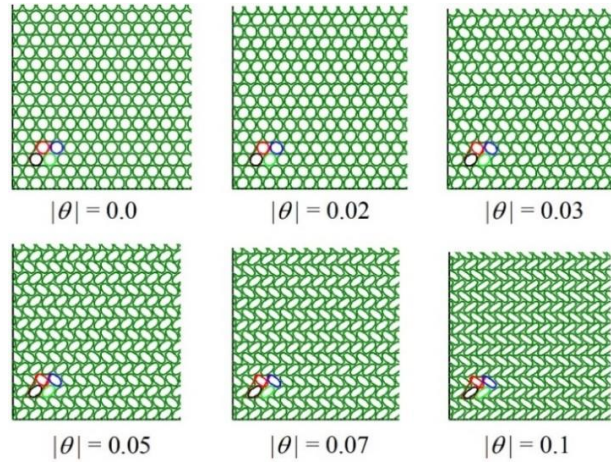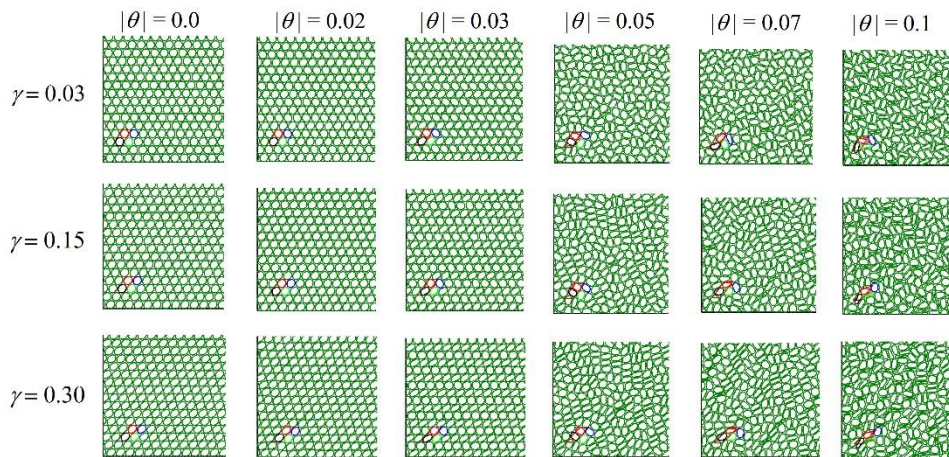

Fig. 2 Structural evolution of CNT bundle at different values of biaxial volumetric strain, θ (presented under each structure). Translation cells of the structures are shown by red lines and includes four CNTs marked for clarity with red, blue, black and light green colors. For a more detailed visualization, only a part (lower left corner) of the computational cell is shown

3.1. Biaxial compression

Fig. 2 demonstrates the evolution of CNT bundle structure subjected to biaxial volumetric strain, θ, along the *x*- and *y*-axes. At strains of $|\theta| < 0.02$, CNTs preserve mainly their circular cross-sections and only small distortions of CNTs, barely visible to the naked eye in the figure, are observed.

An increase of biaxial strain up to $|\theta| = 0.03$ results in an appearance of elliptical cross-sections. At that, as clearly seen in Fig. 2, in the horizontal close-packed rows, the elliptic cross-sections are inclined alternatively in the opposite directions. The latter is the necessary condition to maintain an equilibrium state within the bundle. The straining up to $|\theta| = 0.1$ leads to a further compression of CNTs within the bundle and no collapsed cross-sections are observed. Note that the deformation is performed up to the compressive biaxial volumetric strain $|\theta| \leq 0.1$ to avoid the first-order phase transition related to a formation of the collapsed CNTs, as revealed in Ref. [55].


Fig. 3 Structural evolution of CNT bundle at different values of biaxial volumetric strain, $|\theta|$ (horizontally) and subsequent shear strain, γ (vertically). For a more detailed visualization, only a part (lower left corner) of the computational cell is shown

3.2. Shearing of biaxially pre-strained CNT bundle

The structural evolution of the CNT bundle under biaxial volumetric strain, θ, followed by shear straining is presented in Fig. 3. At low biaxial pre-strains in the range of $|\theta| \leq 0.02$, the deformation is almost uniform, and only small distortions (will be discussed later in more detail) in the form of shear bands in a triangular lattice of CNT bundle are observed at $\gamma = 0.3$. It should be noted that all nanotubes in the computational cell are deformed approximately in the same way, and their cross-sections have the elliptical non-collapsed shape inclined towards the direction of the applied shear strain. An increase of the biaxial pre-strain up to $|\theta| = 0.03$ results in an appearance of longitudinal-transverse shear bands and the nuclei of vortex-like displacements.
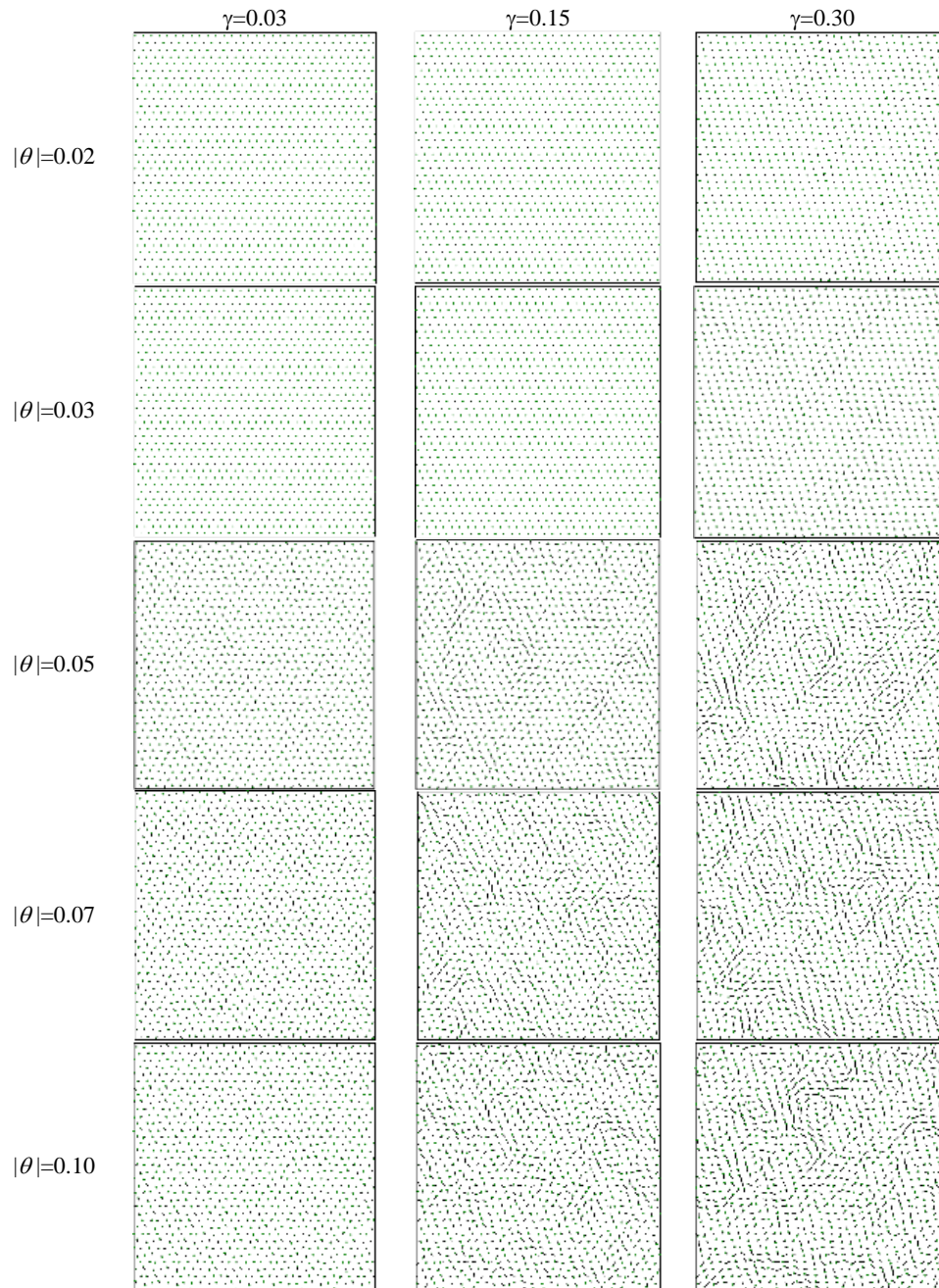
Fig. 4 Displacement field of the centers of mass for each CNT in the computational cell at different values of biaxial volumetric strain, $|\theta|$ (vertically), and shear strain, γ (horizontally)

Moreover, the compression of the horizontal CNT layers becomes inhomogeneous: some layers turn out to be less deformed in contrast to the elements of the neighboring layers, where the deformation is much more pronounced (best seen for $|\theta|=0.03$ and $\gamma = 0.3$). The alternation of such layers with different compression values is to maintain an equilibrium state, which is seen in Fig. 3 for $|\theta|=0.03$. Further increase in biaxial deformation from $|\theta|=0.05$ to 0.1 and subsequent shear result in disordering of the CNT bundle structure. The fraction of collapsed CNTs gradually increases with an increase in biaxial deformation and subsequent shear strain and is maximal at $|\theta| = 0.1$ and $\gamma = 0.3$.

Fig. 4 illustrates the true displacement of the centers of mass of CNTs with respect to the uniformly deformed state. At that, the uniform biaxial compression and shear deformations were subtracted for clarity. At pure shear without preliminary biaxial deformation ($|\theta| = 0.0$), no formation of shear bands or vortices in the structure occurs (not shown in Fig. 4). The same can be said about the case of $|\theta| = 0.02$, as seen, at low biaxial strains, no significant distortions in the structure of CNT bundle are observed. With an increase in the preliminary biaxial deformation, shear bands and vortices begin to appear, which become wider with an increase in the shear strain. The vortices are best seen in Fig. 4 in the structure at $|\theta| = 0.1$ and $\gamma = 0.30$.

Since the average size of vortices is significantly smaller than the size of the computational cell, it can be argued that in this work we consider a representative volume of a CNT bundle.
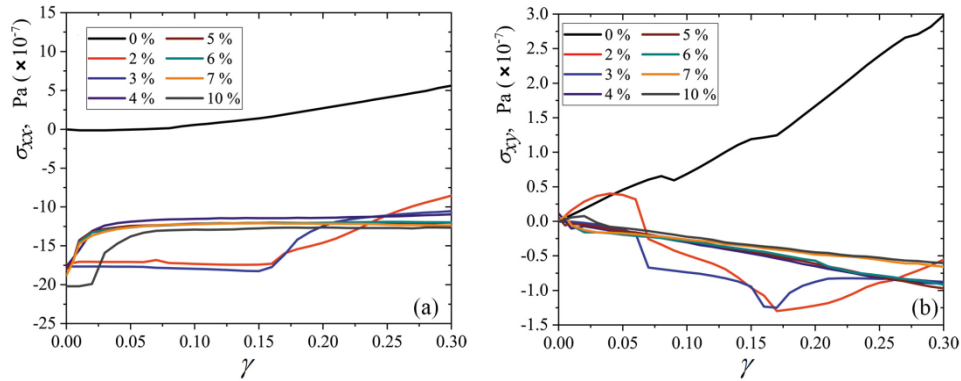

Fig. 5 Dependence of stress components σ_{xx} (a) and σ_{xy} (b) on shear strain, γ at different values of biaxial volumetric strain, $|\theta|$, as indicated in the legends

The structural evolution can be also well seen on the stress-strain curves shown in Fig. 5. The behavior of stress components σ_{xx} and σ_{yy} is very similar, which is expected due to the hexagonal symmetry of the structure, that is why only σ_{xx} is shown in (a). An increase in biaxial compression ($|\theta| > 0.03$) leads to the first increase of both σ_{xx} and σ_{yy} components and saturation at $\gamma = 0.03$, so that σ_{xx} and σ_{yy} practically do not change with increasing shear strain. For all values of $|\theta|$, pressure $p=-(\sigma_{xx} + \sigma_{yy})/2$ decreases with increasing γ. Note that for $|\theta| =0$ for $\gamma > 0$ pressure becomes negative. This means that the CNT bungle with no pre-stress shrinks volumetrically under shear deformation. The behavior of σ_{xy} component is shown in Fig. 5(b). For the structures with $|\theta| > 0.03$, the stresses linearly decrease with

increasing strain as shown in Fig. 5(c). This occurs because the structure of nanotubes initially has a rearranged structure that noticeably differs from the initial one, and due to this, the nucleation of vortex segments occurs already at the compressive state, and the following shear deformation leads to their growth and increase in number. Shear stress for $|\theta|=0$ has the opposite sign as compared to the other values of volumetric strain.

Fig. 6 demonstrates potential energy of the CNT bundle per atom as the function of shear strain for different values of the compressive biaxial volumetric strain (indicated for each curve). In Figs. 6(b) to 6(d), the three components of the potential energy $U=U_B+U_A+U_{VdW}$ are given separately, i.e., the energy of van-der-Waals interactions (U_{VdW}), the energy of valence bonds (U_B) and the energy of valence angles (U_A), respectively.
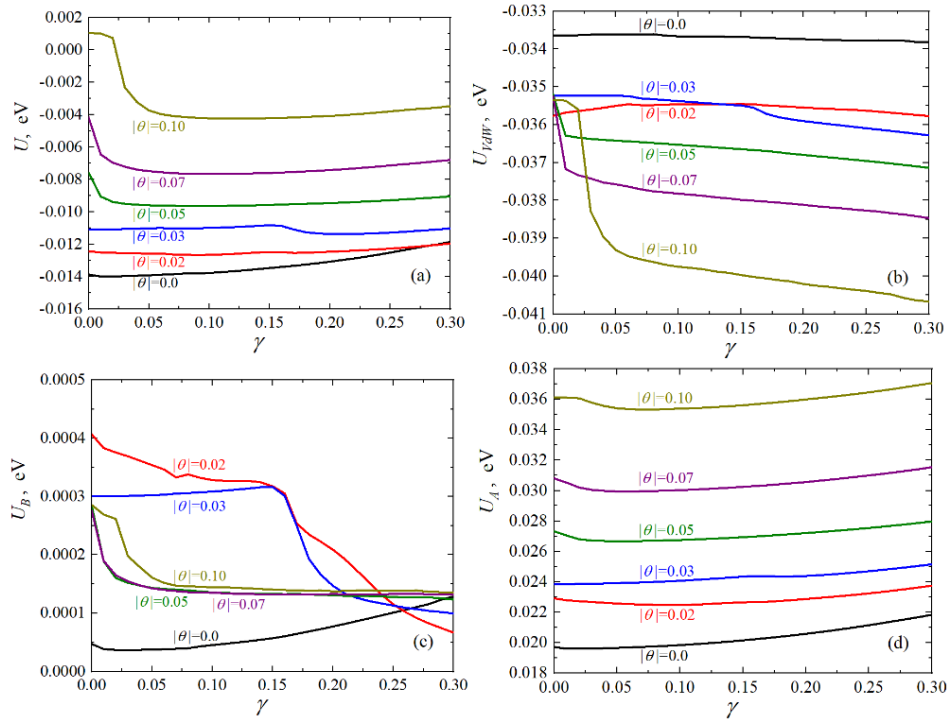
Fig. 6 Potential energy of the CNT bundle per atom as the function of shear strain, γ, calculated for different values of the compressive volumetric strain, $|\theta|$ (indicated for each curve). Total potential energy, $U=U_B+U_A+U_{VdW}$, is shown in (a). Its three components are presented separately: the energy of van-der-Waals interactions, U_{VdW} (b), the energy of valence bonds, U_B (c), and the energy of valence angles, U_A (d)

The energy of the van-der-Waals interactions is negative since it is described by the Lennard-Jones potential with the zero energy level corresponding to well-separated atoms. The creation of the van-der-Waals bonds leads to the reduction of energy below zero. Energies U_B and U_A are positive because for them the zero energy level corresponds to the unstrained flat graphene so that the bending deformation to create a CNT results in an increase of potential energy above zero.

As seen in Fig. 6(b), at $|\theta| \leq 0.03$ the energy of van-der-Waals interactions, U_{VdW}, shows the tendency of a very slow reduction with increasing shear strain. This can be explained by elliptization of CNTs and, as a consequence, an increase in the contact area between adjacent CNT walls, which effectively results in the formation of new van-der-Waals bonds and, therefore, to the reduction of the corresponding energy. At $|\theta|=0.02$, in the range of $\gamma < 0.1$, U_{VdW} slightly increases. This can be a result of the interplay between CNT elliptization, which leads to a decrease of U_{VdW} and pore opening between CNTs due to a better packing under not very high compressive strain. At $|\theta| \geq 0.05$, U_{VdW} decreases with increasing shear strain first very rapidly and then more slowly. This is obviously due to the collapse of CNTs, which leads to the formation of new van-der-Waals bonds between the inner walls of collapsed CNTs.

Fig. 6(c) reveals that the energy stored by valence bonds, U_B, is for two orders of magnitude smaller than the corresponding values of both U_{VdW} and U_A. This is due to very high rigidity of the valence bonds with respect to their tension/compression. One can conclude that the deformation of the CNT bundle occurs mainly due to the bending of the CNT walls and van-der-Waals interactions between CNTs with a negligible contribution from the CNT walls compression or tension.

Fig. 6(d) clearly shows that the energy stored by valence angles, U_A, increases with γ, which is due to elliptization of CNTs growing with shear strain. At $|\theta| \geq 0.05$, a reduction of U_A is seen, when $\gamma < 0.05$. In this initial range of shear strain, collapse of CNTs takes place which frees up the space for non-collapsed CNTs and their cross-sections become closer to circles leading to the net reduction of U_A.

4. CONCLUSIONS

In summary, for the first time, structural evolution of zigzag CNT bundle with the nanotubes of the same diameter under biaxial lateral compression with the subsequent shearing was investigated in the frames of the chain model. Nanotube bundle is a material with highly deformable elements, and, therefore, the deformation mechanisms in them can differ significantly from those typical for conventional polycrystalline or amorphous materials. Simulations revealed that simple biaxial compression results in elliptization of CNT cross sections and formation of the characteristic pattern where CNTs in the horizontal close-packed rows are inclined in the opposite directions. Formation of shear bands and vortex-like displacements in CNT bundle subjected to biaxial pre-straining with subsequent shearing were found. The analysis of the potential energy during shear showed that the energy stored by the valence bonds is for two orders of magnitude smaller than both the energy of van-der-Waals interactions and the energy stored by the valence angles. Thus, the deformation of CNT bundle occurs mainly due to the bending of the CNT walls and van-der-Waals interactions between CNTs play a negligible role.

It should be emphasized that the formation of shear bands is very common for conventional crystalline and amorphous materials, while the formation of vortex-type displacement patterns observed in the present study can be regarded as a new deformation mechanism which can be realized in the material with highly deformable structural units.

Investigation of the effect of the CNT diameter and multi-walled CNTs nanotubes on the deformation behavior and structural evolution may become a natural continuation of the present work. In addition, investigation of CNT bundle with armchair orientation (in

contrast to zigzag orientation studied here) are also of interest for future research. Test calculations show that the chain model used in this work reproduces well the stiffness of the CNT wall in bending and compression, as well as van der Waals interactions; nevertheless, it is important to compare the results reported here with the results of full-atomic modeling, which is planned to be done in one of the future works.

REFERENCES

1. Tersoff, J., Ruoff, R.S., 1994, *Structural properties of a carbon-nanotube crystal*, Phys. Rev. Lett., 73, pp. 676-679.
2. Thess, A., Lee, R., Nikolaev, P., Dai, H., Petit, P., Robert, J., Xu, C., Lee, Y.H., Kim, S.G., Rinzler, A.G., Colbert, D.T., Scuseria, G.E., Tomanek, D., Fischer, J.E., Smalley, R.E., 1996, *Crystalline ropes of metallic carbon nanotubes*, Science, 273, pp. 483-487.
3. Saether, E., Frankland, S.J.V., Pipes, R.B., 2003, *Transverse mechanical properties of single-walled carbon nanotube crystals. Part I: Determination of elastic moduli*, Compos. Sci. Technol., 63, pp. 1543-1550.
4. Rakov, E.G., 2013, *Materials made of carbon nanotubes. The carbon nanotube forest*, Russ. Chem. Rev., 82, pp. 538-566.
5. Samsonidze, G.G., Samsonidze, G.G., Yakobson, B.I., 2002, *Kinetic theory of symmetry-dependent strength in carbon nanotubes*, Phys. Rev. Lett., 88, 065501.
6. Shenderova, O.A., Zhirnov, V.V., Brenner, D.W., 2002, *Carbon nanostructures*, Crit. Rev. Solid State, 27, pp. 227-356.
7. Yu, M.-F., 2004, *Fundamental mechanical properties of carbon nanotubes: Current understanding and the related experimental studies*, J. Eng. Mater. T. ASME, 126, pp. 271-278.
8. Yu, M.-F., Lourie, O., Dyer, M.J., Moloni, K., Kelly, T.F., Ruoff, R.S., 2000, *Strength and breaking mechanism of multiwalled carbon nanotubes under tensile load*, Science, 287, pp. 637-640.
9. Yu, M.-F., Files, B.S., Arepalli, S., Ruoff, R.S., 2000, *Tensile loading of ropes of single wall carbon nanotubes and their mechanical properties*, Phys. Rev. Lett., 84, pp. 5552-5555.
10. Dhanabalan, S.C., Dhanabalan, B., Chen, X., Ponraj, J.S., Zhang, H., 2019, *Hybrid carbon nanostructured fibers: Stepping stone for intelligent textile-based electronics*, Nanoscale, 11, pp. 3046-3101.
11. Bai, Y.,, Zhang, R., Ye, X., Zhu, Z., Xie, H., Shen, B., Cai, D., Liu, B., Zhang, C., Jia, Z., Zhang, S., Li, X., Wei, F., 2018, *Carbon nanotube bundles with tensile strength over 80 GPa*, Nat. Nanotechnol., 13, pp. 589-595.
12. Qiu, L., Wang, X., Tang, D., Zheng, X., Norris, P.M., Wen, D., Zhao, J., Zhang, X., Li, Q., 2016, *Functionalization and densification of inter-bundle interfaces for improvement in electrical and thermal transport of carbon nanotube fibers*, Carbon, 105, pp. 248-259.
13. Cho, H., Lee, H., Oh, E., Lee, S.-H., Park, J., Park, H.J., Yoon, S.-B., Lee, C.-H., Kwak, G.-H., Lee, W.J., Kim, J., Kim, J.E., Lee, K.-H., 2018, *Hierarchical structure of carbon nanotube fibers, and the change of structure during densification by wet stretching*, Carbon, 136, pp. 409-416.
14. Fernández-Toribio, J.C., Alemán, B., Ridruejo, Á., Vilatela, J.J., 2018, *Tensile properties of carbon nanotube fibres described by the fibrillar crystallite model*, Carbon, 133, pp. 44-52.
15. Dang, Z.-M., Yuan, J.-K., Zha, J.-W., Zhou, T., Li, S.-T., Hu, G.-H., 2012, *Fundamentals, processes and applications of high-permittivity polymer-matrix composites*, Prog. Mater. Sci., 57, pp. 660-723.
16. Bakshi, S.R., Lahiri, D., Agarwal, A., 2010, *Carbon nanotube reinforced metal matrix composites - A review*, Int. Mater. Rev., 55, pp. 41-64.
17. Dorri-Moghadam, A., Omrani, E., Menezes, P.L., Rohatgi, P.K., 2015, *Mechanical and tribological properties of self-lubricating metal matrix nanocomposites reinforced by carbon nanotubes (CNTs) and graphene - A review*, Compos. Part B: Eng., 77, pp. 402-420.
18. Gondane, S., Singh, A.K., Sinha, N., Vijayakumar, R.P., 2020, *Experimental study on steady dynamic friction of MWCNTs mixed lubricants*, Surf. Rev. Lett., 27(7), 1950172.
19. Reinert, L., Lasserre, F., Gachot, C., Grützmacher, P., Maclucas, T., Souza, N., Mücklich, F., Suarez, S., 2017, *Long-lasting solid lubrication by CNT-coated patterned surfaces*, Sci. Rep., 7, 42873.

20. Singh, H., Bhowmick, H., 2020, *Lubrication characteristics and wear mechanism mapping for hybrid aluminium metal matrix composite sliding under surfactant functionalized MWCNT-oil*, Tribol. Int., 145, 106152.

21. Cao, A.Y., Dickrell, P.L., Sawyer, W.G., Ghasemi-Nejhad, M.N., Ajayan, P.M., 2005, *Super-compressible foamlike carbon nanotube films*, Science, 310, pp. 1307-1310.

22. Pathak, S., Kalidindi, S.R., 2015, *Spherical nanoindentation stress-strain curves*, Materials Science and Engineering R: Reports, 91, pp. 1-36.

23. Pathak, S., Cambaz, Z.G., Kalidindi, S.R., Swadener, J.G., Gogotsi, Y., 2009, *Viscoelasticity and high buckling stress of dense carbon nanotube brushes*, Carbon, 47, pp. 1969-1976.

24. Maschmann, M.R., Zhang, Q., Du, F., Dai, L., Baur, J., 2011, *Length dependent foam-like mechanical response of axially indented vertically oriented carbon nanotube arrays*. Carbon, 49, pp. 386-397.

25. Cao, C., Reiner, A., Chung, C., Chang, S.-H., Kao, I., Kukta, R.V., Korach, C.S., 2011, *Buckling initiation and displacement dependence in compression of vertically aligned carbon nanotube arrays*, Carbon, 49, pp. 3190-3199.

26. Liang, X., Shin, J., Magagnosc, D., Jiang, Y., Jin Park, S., John Hart, A., Turner, K., Gianola, D.S., Purohit, P.K., 2017, *Compression and recovery of carbon nanotube forests described as a phase transition*, Int. J. Solids Struct., 122-123, pp. 196-209.

27. Koumoulos, E.P., Charitidis, C.A., 2017, *Surface analysis and mechanical behaviour mapping of vertically aligned CNT forest array through nanoindentation*, Appl. Surf. Sci., 396, pp. 681-687.

28. Pour Shahid Saeed Abadi, P., Hutchens, S.B., Greer, J.R., Cola, B.A., Graham, S., 2013, *Buckling-driven delamination of carbon nanotube forests*, Appl. Phys. Lett., 102, 223103.

29. Silva-Santos, S.D., Alencar, R.S., Aguiar, A.L., Kim, Y.A., Muramatsu, H., Endo, M., Blanchard, N.P., San-Miguel, A., Souza Filho, A.G., 2019, *From high pressure radial collapse to graphene ribbon formation in triple-wall carbon nanotubes*, Carbon, 141, pp. 568-579.

30. Tangney, P., Capaz, R.B., Spataru, C.D., Cohen, M.L., Louie, S.G., 2005, *Structural transformations of carbon nanotubes under hydrostatic pressure*, Nano Lett., 5, pp. 2268-2273.

31. Zhang, S., Khare, R., Belytschko, T., Hsia, K.J., Mielke, S.L., Schatz, G.C., 2006, *Transition states and minimum energy pathways for the collapse of carbon nanotubes*, Phys. Rev. B, 73, 075423.

32. Shima, H., Sato, M., 2008, *Multiple radial corrugations in multiwalled carbon nanotubes under pressure*, Nanotechnology, 19, 495705.

33. Zhao, Z.S., Zhou, X.-F., Hu, M., Yu, D.L., He, J.L., Wang, H.-T., Tian, Y.J., Xu, B., 2012, *High-pressure behaviors of carbon nanotubes*, J. Superhard Mater., 34, pp. 371-385.

34. Islam, S., Saleh, T., Asyraf, M.R.M., Mohamed Ali, M.S., 2019, *An ex-situ method to convert vertically aligned carbon nanotubes array to horizontally aligned carbon nanotubes mat*, Mater. Res. Express, 6, 025019.

35. Zhang, R., Zhang, Y., Wei, F., 2017, *Horizontally aligned carbon nanotube arrays: Growth mechanism, controlled synthesis, characterization, properties and applications*, Chem. Soc. Rev., 46, pp. 3661-3715.

36. Nam, T.H., Goto, K., Yamaguchi, Y., Premalal, E.V.A., Shimamura, Y., Inoue, Y., Naito, K., Ogihara, S., 2015, *Effects of CNT diameter on mechanical properties of aligned CNT sheets and composites*, Compos. Part A: Appl. S., 76, pp. 289-298.

37. Qiu, L., Wang, X., Su, G., Tang, D., Zheng, X., Zhu, J., Wang, Z., Norris, P.M., Bradford, P.D., Zhu, Y., 2016, *Remarkably enhanced thermal transport based on a flexible horizontally-aligned carbon nanotube array film*, Sci. Rep., 6, 21014.

38. Tang, J., Sasaki, T., Yudasaka, M., Matsushita, A., Iijima, S., 2000, *Compressibility and polygonization of single-walled carbon nanotubes under hydrostatic pressure*, Phys. Rev. Lett., 85, pp. 1887-1889.

39. Karmakar, S., Sharma, S.M., Teredesai, P.V., Muthu, D.V.S., Govindaraj, A., Sikka, S.K., Sood, A.K., 2003, *Structural changes in single-walled carbon nanotubes under non-hydrostatic pressures: X-ray and Raman studies*, New J. Phys., 5, pp. 143.1-143.11.

40. Wittmaack, B.K., Volkov, A.N., Zhigilei, L.V., 2019, *Phase transformation as the mechanism of mechanical deformation of vertically aligned carbon nanotube arrays: Insights from mesoscopic modeling*, Carbon, 143, pp. 587-597.

41. Wittmaack, B.K., Volkov, A.N., Zhigilei, L.V., 2018, *Mesoscopic modeling of the uniaxial compression and recovery of vertically aligned carbon*, Compos. Sci. Technol., 166, pp. 66-85.

42. Yakobson, B.I., Brabec, C.J., Bernholc, J., 1996, *Nanomechanics of carbon tubes: Instabilities beyond linear response*, Phys. Rev. Lett., 76, pp. 2511-2514.

43. Impellizzeri, A., Briddon, P., Ewels, C.P., 2019, *Stacking- and chirality-dependent collapse of single-walled carbon nanotubes: A large-scale density-functional study*, Phys. Rev. B, 100, 115410.

44. Chopra, N.G., Benedict, L.X., Crespi, V.H., Cohen, M.L., Louie, S.G., Zettl, A., 1995, *Fully collapsed carbon nanotubes*, Nature, 377, pp. 135-138.

45. Chang, T., 2008, *Dominoes in carbon nanotubes*, Phys. Rev. Lett., 101, 175501.
46. Ji, J., Zhao, J., Guo, W., 2019, *Novel nonlinear coarse-grained potentials of carbon nanotubes*, J. Mech. Phys. Solids, 128, pp. 79-104.
47. Savin, A.V., Korznikova, E.A., Dmitriev, S.V., 2015, *Scroll configurations of carbon nanoribbons*, Phys. Rev. B, 92, 035412.
48. Savin, A.V., Korznikova, E.A., Dmitriev, S.V., 2015, *Simulation of folded and scrolled packings of carbon nanoribbons*, Phys. Solid State, 57, pp. 2348-2355.
49. Savin, A.V., Korznikova, E.A., Lobzenko, I.P., Baimova, Y.A., Dmitriev, S.V., 2016, *Symmetric scrolled packings of multilayered carbon nanoribbons*, Phys. Solid State, 58, pp. 1278-1284.
50. Savin, A.V., Korznikova, E.A., Dmitriev, S.V., Soboleva, E.G., 2017, *Graphene nanoribbon winding around carbon nanotube*, Comp. Mater. Sci., 135, pp. 99-108.
51. Savin, A.V., Mazo, M.A., 2019, *2D chain models of nanoribbon scrolls*, Adv. Struct. Mat., 94, pp. 241-262.
52. Savin, A.V., Korznikova, E.A., Dmitriev, S.V., 2019, *Dynamics of surface graphene ripplocations on a flat graphite substrate*, Phys. Rev. B, 99, 235411.
53. Korznikova, E.A., Rysaeva, L.K., Savin, A.V., Soboleva, E.G., Ekomasov, E.G., Ilgamov, M.A., Dmitriev, S.V., 2019, *Chain model for carbon nanotube bundle under plane strain conditions*, Materials, 12(23), 3951.
54. Rysaeva, L.K., Korznikova, E.A., Murzaev, R.T., Abdullina, D.U., Kudreyko, A.A., Baimova, J.A., Lisovenko, D.S., Dmitriev, S.V., 2020, *Elastic damper based on the carbon nanotube bundle*, Facta Universitatis-Series Mechanical Engineering, 18(1), pp. 1-12.
55. Abdullina, D.U., Korznikova, E.A., Dubinko, V.I., Laptev, D.V., Kudreyko, A.A., Soboleva, E.G., Dmitriev, S.V., Zhou, K., 2020, *Mechanical response of carbon nanotube bundle to lateral compression*, Computation, 8(2), 27.
56. Savin, A.V., Kivshar, Y.S., Hu, B., 2010, *Suppression of thermal conductivity in graphene nanoribbons with rough edges*, Phys. Rev. B, 82, 195422.
57. Savin, A.V., Korznikova, E.A., Krivtsov, A.M., Dmitriev, S.V., 2020, *Longitudinal stiffness and thermal conductivity of twisted carbon nanoribbons*, Eur. J. Mech. A-Solid., 80, 103920.
58. Savin, A.V., 2019, *Thermal rectifiers based on asymmetric interaction of molecular chains, carbon nanoribbons, and nanotubes with thermostats*, Phys. Rev. B, 10, 245415.
59. Shcherbinin, S.A., Semenova, M.N., Semenov, A.S., Korznikova, E.A., Chechin, G.M., Dmitriev, S.V., 2019, *Dynamics of a three-component delocalized nonlinear vibrational mode in graphene*, Phys. Solid State, 61, pp. 2139-2144.
60. Abdullina, D.U., Semenova, M.N., Semenov, A.S., Korznikova, E.A., Dmitriev, S.V., 2019, *Stability of delocalized nonlinear vibrational modes in graphene lattice*, Eur. Phys. J. B, 92, 249.
61. Savin, A.V., Korznikova, E.A., Dmitriev, S.V., 2019, *Improving bending rigidity of graphene nanoribbons by twisting*, Mech. Mater., 137, 103123.